ARMA 17-174

Insight into Hard Rock Pillar Behavior from Numerical Simulation Using a Progressive S-Shaped Failure Criterion

Sinha, Sankhaneel
Colorado School of Mines, Golden, Colorado, USA.
Walton, Gabriel
Colorado School of Mines, Golden, Colorado, USA.

This paper was prepared for presentation at the 51st US Rock Mechanics / Geomechanics Symposium held in San Francisco, California, USA, 25-28 June 2017. This paper was selected for presentation at the symposium by an ARMA Technical Program Committee based on a technical and critical review of the paper by a minimum of two technical reviewers. The material, as presented, does not necessarily reflect any position of ARMA, its officers, or members. Electronic reproduction, distribution, or storage of any part of this paper for commercial purposes without the written consent of ARMA is prohibited. Permission to reproduce in print is restricted to an abstract of not more than 200 words; illustrations may not be copied. The abstract must contain conspicuous acknowledgement of where and by whom the paper was presented.

ABSTRACT: In recent decades, several researchers have found that the behavior of brittle rocks near excavation boundaries under intermediate to high stress conditions is best described by a Cohesion-Weakening-Friction-Strengthening (CWFS) Model. The advantage of CWFS over conventional shear strength failure criterions in describing the process of extensile fracturing (spalling) makes it ideal for modelling damage processes in hard rock pillars. The majority of numerical studies of pillars to date, however, have focused on the application of strain-softening material models; while these models may be suitable for capturing mine-scale behavior of pillar systems, they provide little insight into the mechanisms governing pillar stability. Recently, the concept of an S-shaped strength criterion was introduced which combined the CWFS strength model (at low confining stress) with the classical shear strength envelopes (at higher confining stress). Theoretically, such a model should better capture the brittle fracturing phenomenon along the ribs and the shear fracturing inside the pillar where confinement is high. In this study, the progressive S-shaped strength envelope has been implemented in FLAC^{3D} using a bilinear strength model and has been demonstrated to exhibit some well-documented behavior seen in failing pillars. As a final step, a range of width/height ratios were tested and the results were compared against published field data, empirical strength envelopes, and previous modelling attempts presented in the literature.

1. INTRODUCTION

With underground mining extending to depths over 2 kms, it is essential to design stable pillars which can provide local as well as regional support [1]. Pillar design is based on two important parameters – strength and applied stress, both of which are difficult to estimate analytically. Numerical modelling offers a convenient alternative to estimate these quantities, and is often employed during the design phase of a project. The success of such modelling is governed by the selection of a proper constitutive model and associated input parameters.

In this paper, an attempt is made to develop a local constitutive relationship that can account for micromechanical damage processes while exhibiting emergent macroscopic failure behavior in rock pillars. The developed constitutive relationship, termed as the progressive S-shaped failure criterion in this study, is first tested for its ability to qualitatively capture observed rock damage processes using a pillar model in FLAC^{3D}, followed by comparison against an empirical pillar strength database from literature.

Ground failures in hard rock excavations depend primarily on the in-situ stress magnitude and the degree of rock jointing [2]. In massive to sparsely fractured rock under high stress conditions, damage near excavations is dominated by extensile fractures parallel to the boundary often termed as spalling [3,4,5,6]. The extensile fracturing process is essentially a cohesion loss process followed by frictional mobilization [7,8]. The conventional shear strength based models like Hoek-Brown and Mohr-Coulomb assume simultaneous mobilization of friction and cohesion and thus cannot describe the brittle failure process [6]. Attempts to model the onset of brittle fracturing and extent of damage using these conventional models were unsuccessful in the past [6,9,10].

Based originally on the idea of Schmertermann and Osterberg [11], a Cohesion-Weakening-Friction-Strengthening (CWFS) model was formally introduced by Hajiabdolmajid et al.[10] in the last decade. Figure 1 shows a conceptual model of CWFS. This strain-dependent strength criterion accounts for the non-simultaneous mobilization of friction and cohesion. However, the behavior of a rock pillar cannot be simulated using only CWFS. This is because the extensile fracturing process is restricted only to the boundary of excavations where the level of confining

stress is low. Away from the excavation boundary, the confining stress is higher, which suppresses the development and propagation of these fractures [4]. As a result, the peripheral portion of a pillar exhibits CWFS behavior while central portion fails though a shear mechanism.

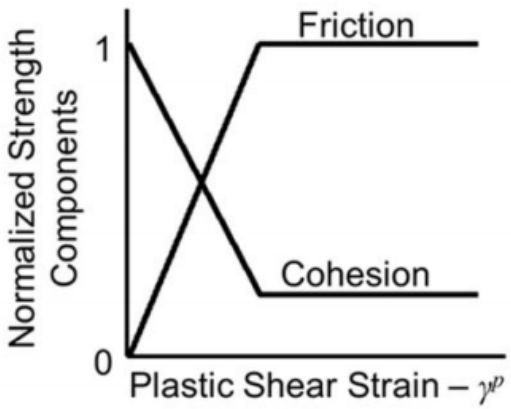

Figure 1: Conceptualized CWFS strength model [12].

A pillar subjected to continually increasing load (for eg. during sequential excavation of stopes) exhibits five failure stages [13]:

- No fractures,
- Slight spalling of pillar corners and pillar walls,
- One or few fractures near surface with distinct spalling,
- Fracturing in central parts of the pillars,
- One or a few fractures occurring through central parts of the pillar, dividing it into two or several parts, and,
- Disintegration of the pillar forming a well-developed hour-glass shape with central part completely crushed.

Krauland and Soder [13] based these stages on field observations. A proper constitutive model should be able to exhibit most of these stages numerically. To the knowledge of the authors, no studies have previously compared such a model against the behavioral aspects of a failing pillar. The developed finite difference model will be shown to indeed have the capability of displaying some of these widely accepted failure behaviors.

There are several numerical studies which have attempted to reproduce hard rock pillar behavior using Hoek-Brown [14], Mohr-Coulomb [15] and CWFS [16]. The studies which employed the classical shear strength envelopes (Hoek-Brown and Mohr-Coulomb) predicted very high normalized pillar strength values in the range of 0.7-1.0 for W/H ratio >2. Such an observation is in direct contradiction with the empirical pillar strength data (see section 5). The authors believe that the reason for such a discrepancy is the improper selection of a constitutive model. Brittle H-B parameters (m_b=0 and s=0.11), although capable of describing extensile spalling failure, cannot account for the shear failure mechanism inside a pillar.

Walton et al. [16] performed a back analysis of a hard rock case study of the Creighton mine (Sudbury, Canada) using only a CWFS strength model in association with a mobilized dilation angle model [17]. Interestingly, this model could illustrate some of the well-documented pillar behavior (e.g. increase in the confining stress at the pillar core following yield, hardening of stress-strain curve in the pre-peak region, etc.). The model also demonstrated the formation and extension of cracks which was confirmed by extensometer measurements. Since the calibrated parameters from this study were well constrained, they were selected as a starting point for the numerical models presented in this paper. The logical question that arises here is whether a CWFS strength model can capture rock pillars behavior independent of any consideration of shear deformation mechanisms. The answer lies in the low aspect ratio of the Creighton mine pillars. Since the W/H was about 1.5, the effect of confinement and shear failure was not significant. It will be demonstrated in this study that the S-shaped criterion stands out particularly for squat pillars.

For the case of pillars with larger W/H ratios, the authors hypothesize the need to use a progressive (i.e. evolving) tri-linear strength envelope that honors the varying failure mechanisms in the different confinement regimes. Only in the last decade, a theoretical S-shaped failure envelope was conceived by Diederichs [4] and formalized by Kaiser et. al [18] and Kaiser and Kim [19] which coupled the CWFS at low confinement and shear strength envelope at high confinement (see Figure 2). One aspect that was not properly addressed in these precursory works is the importance of the evolutionary nature of the envelope. It is not sufficient to capture the tri-linear shape of only the ultimate strength envelope; the complete strength envelope must be defined for all material states (e.g. with respect to material damage). This reason is that the complex interrelationships between the mobilization of cohesion, friction, and dilation ultimately control pillar behavior. Without accounting for the evolution of these parameters, small-scale damage and stress re-distribution processes are not captured properly.

It is a common notion that the strength of a pillar is functionally related to the shape, size and the aspect ratio i.e. width/height [20,21,22,23,24]. The relationships derived through several studies are based on field observations and subjective classification of pillar stability. For determination of the failure stress, historically used methods ranged from simple tributary area theory to more complex two and three dimensional modeling. Among the proposed empirical relationships and previous modeling attempts, there exist a major disparity

regarding the extent of pillar hardening beyond an aspect ratio of 2. Lunder and Pakalnis [22] and Hedley and Grant [21] showed that the strength of pillars level down beyond a W/H of 2. Martin and Maybee [14] and Mortazavi et al. [15], on the other hand, found a near-exponential increase in strength from their numerical models. Further investigation is required to assess why numerical models were unsuccessful in capturing pillar strengths at high W/H.

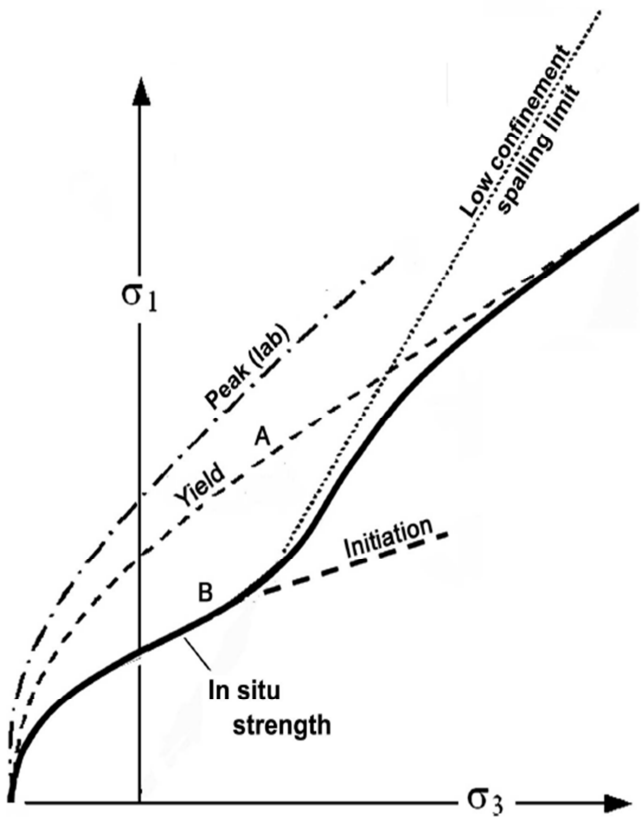

Figure 2: Evolving S-shaped strength envelope [4].

2. DEVELOPMENT OF A PROGRESSIVE S-SHAPED FAILURE CRITERION

As previously discussed, a CWFS strength model alone cannot completely describe the damage processes in a pillar. A realistic pillar constitutive model should exhibit two fundamental behaviors: a) a decrease in cohesion and increase in angle of friction at low confinement (CWFS behavior), and b) a simultaneous decrease in friction angle and cohesion at high confinement (shear failure). This evolving behavior is dependent on the amount of damage incurred to the system.

The term 'damage' has been quantified in numerous ways by different authors. Since there is no such universal parameter, plastic shear strain (γ^p) is often chosen due to its associated advantages [10,12,16,25,27,27]: this parameter can be easily measured in the laboratory and can also be related to the incremental plastic parameter (ε^{ps}) in FLAC^{3D} using a simple relationship $\epsilon^{ps} = \frac{1}{2}\gamma^p$ [12].

In this section, the two components of the S-shaped criterion, namely the CWFS portion and the shear failure portion, are presented individually first; then they are combined and discussed thereafter:

(a) In CWFS strength model, the initial yield curve is coincident with the Crack Initiation (CI) threshold, while the residual curve corresponds to the spalling limit. For a particular rock type, the Crack Initiation (CI) threshold can be identified using acoustic emission techniques [28], volumetric stress-strain curves [29] and/or axial/lateral stress-strain curves [4,30,31]. The spalling limit was suggested by Diederichs [4] to be σ_1/σ_3=10-20 , and describes the ultimate strength of spalled ground at low confinement (more specifically it is the residual strength at very low confinement and peak strength at moderate confinement). Under low confinement conditions, CI acts as the initial point of yield in-situ; however, recent laboratory testing work suggests that under higher confining stresses, when the failure mechanism begins to transition towards semi-ductile shear, the initial yield is governed by Mogi's line [32,33]. Mechanistically this re-emphasizes the fact that when confinement is high, the stable crack formation and subsequent lateral dilation is suppressed resulting in an initial yield strength higher than the CI.

(b) Crack Damage (CD) defines the ultimate strength envelope for high confinement conditions where the predominant mode of failure is through shear mechanism. It has been experimentally established that compressive strengths, as measured in laboratory, are a function of the loading conditions and specimen geometry; the true long-term strength is actually coincident with CD [8]. Since pillar loading is a very slow phenomenon, the CD envelope serves to better represent the shear strength rather than the peak envelope obtained from uniaxial and triaxial tests in laboratory. Post-failure, the CD threshold is gradually degraded to a residual value which is a common characteristic of classical shear strength criteria.

Figure 3 illustrates the complete S-shaped envelope. Some of the important features of this composite envelope are as follows:

- The left portion of the initial yield envelope (red dotted line), corresponding to an eps of 0, is the CI envelope while the right portion is the Mogi's line. The CI limits the maximum attainable strength at very low confinement.
- The left portion of the mobilized strength envelope (blue dotted line) corresponds to spalling limit while the right portion follows CD.

- The residual envelope (black solid line) was included to denote the gradual reduction of friction and cohesion which occurs after initial brittle strength loss/mobilization. The reader is referred to Martin[6] for additional details on the low confinement portion of the residual envelope.
- Below a confinement of 45 MPa (point of intersection of the CI and Mogi's line), the envelope exhibits a CWFS behavior. On the other hand, beyond 45 MPa, the behavior is identical to a shear yield model where the strength envelope degrades from peak to residual following yield.
- The residual curve exceeds the peak curve (e.g. strain-hardening) beyond a confinement level of 150 MPa. This observation has been confirmed through laboratory experiments [32].
- The tri-linear shape of the upper (ultimate) envelope conforms well to the S-shaped strength envelope proposed by Diederichs [4], Kaiser et al. [18] and Kaiser and Kim [19].

For the modeling exercise performed as part of this study, the calibrated parameters of Walton et al. [16] were chosen as the starting point. Only CD was not available for the particular rock type used (Creighton Granite); so an approximate value was selected after a review of laboratory stress-strain curves for similar rock types. Table 1 lists the different thresholds used in developing the failure criterion. It must be mentioned here that the entire study was conducted in FLAC^{3D} and as a result, the bilinear shape of each segment of the evolving envelope corresponding to particular eps values was constrained by the available constitutive models built into FLAC^{3D}.

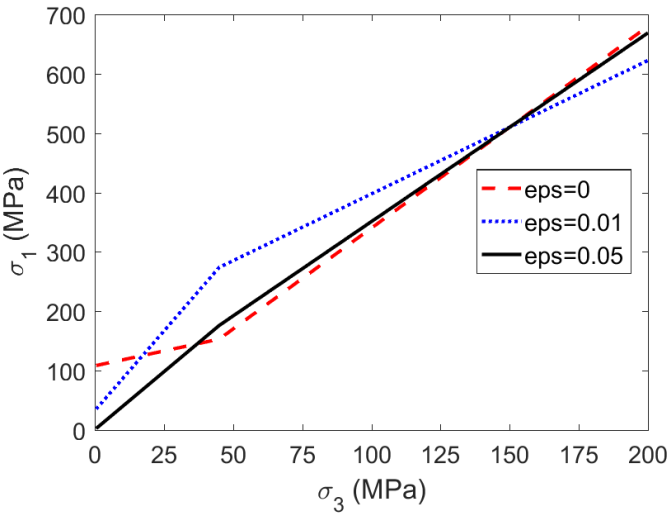

Figure 3: Progressive S-shaped strength criterion (red indicates yield, blue indicates peak and black indicates residual).

An important topic that has not been discussed previously is the role of dilation in the damage processes within a pillar. With the onset of inelastic deformation, inelastic lateral strains develop which in turn increases the confinement and the strength of neighboring elements. Although localized, this phenomenon can significantly affect the global behavior of rock pillars. The magnitude of the lateral plastic strain is controlled by the parameter dilation angle which mathematically relates the plastic axial and lateral strain [12]. Several studies have found that the dilation angle is a function of confining stress and plastic shear strain and can be better represented by a mathematical model [17,34,35,36]. Accounting for this mobilized nature of dilation angle is necessary for completely capturing the micro-damage processes within a pillar.

3. MODEL DEVELOPMENT

The S-shaped failure criterion was numerically implemented using the bilinear strain-softening ubiquitous joint constitutive model in FLAC^{3D}. An 8m x 8m x 8m cubic pillar model with mesh size of 0.166m x 0.166m x 0.166m was developed and loaded quasi-statically (displacement boundary condition) through two elastic beams on either side (Figure 4). The elastic constants and dilation parameters are listed in Table 2 while the rockmass parameters can be computed from Table 1 using Equations (i) and (ii):

$$c = \frac{\sigma_c*(1-sin\,\varphi)}{2*cos\varphi} \quad \text{(i)}$$

$$\varphi = sin^{-1}(\frac{k-1}{k+1}) \quad \text{(ii)}$$

where c is cohesion, φ is angle of friction, σ_c is the uniaxial compressive strength (constants in Table 1) and k is the slope in σ_1-σ_3 space (multiplier of σ_3 in Table 1). The reader is referred to Walton and Diederichs [17,34] for details on selection of mobilized dilation angle input parameters.

The bilinear strain-softening ubiquitous-joint model in FLAC^{3D} has the capability of simulating planes of weaknesses along a user-defined direction. This could be used for assessing the effect of joints orientation on the macro-behavior of pillar; however, for the purposes of this study, extremely large strength values were assigned to these joint parameters.

Table 1: Mathematical representation of the thresholds in σ_1-σ_3 space.

Segments of the S-shaped envelope	Threshold in σ_1-σ_3 space
CI	σ_1-σ_3=110
CD	σ_1-2.25*σ_3=173
Spalling Limit	σ_1-5.4*σ_3=32.5
Residual (left)	σ_1-3.90*σ_3=0.40
Residual (right)	σ_1-3.2*σ_3=33

Some may assume that the plastic shear strain corresponding to the degradation of cohesion and mobilization of friction is an intrinsic property of the material and remains constant for all mesh sizes. When numerically implemented (e.g. in FLAC^{3D}), however, the pre-peak and post-peak behavior is highly sensitive to the selected mesh size [37]. An approach proposed by Itasca [37] is to recalibrate a model if the mesh element size is varied. However, recalibration was not a feasible option here because of the hypothetical nature of the study. As a viable alternative, a linear conversion factor [37] of 1.9 (mesh size in Walton et al. [16] was 0.3125 m in comparison to 0.166 m in this study) was chosen to approximately account for this grid dependency.

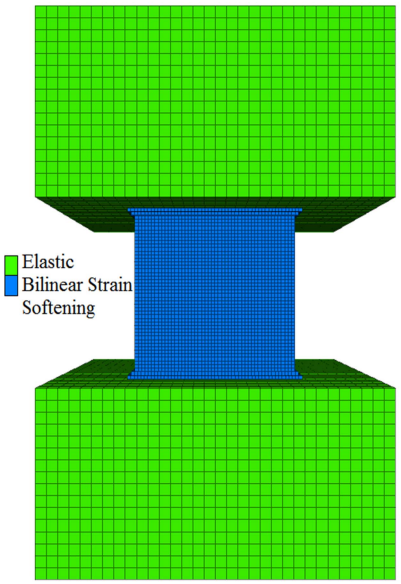

Figure 4: Pillar model developed for this study in FLAC^{3D}.

Table 2: Rock mass and dilation parameters used in model.

Parameter	Value assigned in the model
Young's Modulus (MPa)	80 GPa
Poisson's ratio	0.1
Plastic shear strain to mobilized strength envelope	0.01
Plastic shear strength to residual envelope	0.05
Mobilized dilation angle model inputs	
Pre-mobilization Parameter (α_0)	0.001
Pre-mobilization Confinement Dependence (α')	0.0038
Dilation Mobilization Plastic Shear strain (e^{ps}_m)	0.0015
Low Confinement Peak Dilation Parameter (β_0)	1.1
High Confinement Peak Dilation Parameter (β')	0.14
Dilation Decay Parameter (e^{ps*})	0.01

The geometry and loading conditions were finalized after testing a large number of different model setups. Some of the most relevant findings from this exercise are as follows:

- Loading rate: It was decided to apply a constant vertical velocity of $5x10^{-8}$ m/step on either end of the elastic beam. Simulations showed a negligible effect of loading rate below this value on the peak strength and the post-peak portion of the pillar stress-strain curve.
- Traditional CWFS versus S-shaped criterion: S-shaped criterion was chosen due to complete representation of the low-confinement extensile fracturing process as well as the high confinement shear failure mechanisms.
- Constant dilation angle versus mobilized dilation angle (W-D): The use of a constant dilation angle predicted unrealistic confinement (resulting in excessive load carrying capacity) around the core of the pillar. The dilation model proposed by Walton and Diederichs[17] was thus used to simulate the confinement and damage dependency of dilatancy.
- Direct loading versus beam loading: Some of the models failed to converge when the pillar was loaded directly. The instability was due to excessive concentration of displacements and velocity within some of the boundary elements. The problem was resolved when an elastic beam was used instead.
- Mesh size, beam dimension and constitutive model of the beams: A detailed sensitivity analysis was conducted varying mesh size, beam dimension and constitutive models. Results indicated a practically negligible effect of these variables on the damage processes in the pillar. To keep the model run-time manageable, an 16m x 16m x 8m elastic beam with 0.5m x 0.5m x 0.5m mesh was selected. Additionally, identical elastic properties were assigned to the pillar and the beams to eliminate any end-effects.
- Rounded versus non-rounded pillar corners: Pillar simulations with non-rounded and various degree of rounding indicated that the sensitivity of the results to the rounding used beyond two element rounding was relatively small. Additionally, a two element rounded pillar seemed to reasonably approximate the typical shape of pillars seen in-situ.

FLAC^{3D} has a built-in programming language FISH that enables users to define new functions and plot different variables. Using the FISH language, two functions were developed to record the displacement and stress changes in the pillar. The functions were designed to loop over every element in the pillar and store the stresses and displacements in a table for that corresponding solution

step. This is a memory-intensive operation; to keep the runtime manageable and obtain an acceptable data resolution, the functions were called every 1000 solution steps.

This study is only a demonstration of the efficacy of the progressive S-shaped failure criterion. The developed numerical models were checked for consistency with empirical observations by correlating the outputs with the pillar strength curve in literature, the hourglass shape of the load-bearing pillar core [13] and the development of stresses along the mid-section of the pillar [38]. The authors feel that the robustness of the constitutive relationship in explaining the micromechanical and the macro-damage processes in a pillar can be fairly substantiated on the basis of these assessments.

4. MODEL RESULTS AND ANALYSIS

Eight (8) cases (corresponding to W/H=0.5, 1, 1.5, 2, 2.5, 3,3.5 and 4) in total were run using the model setup described in the previous section. To ensure that the global pillar strength was captured in each of the cases, the simulations were run for a sufficient number of solution steps. The number of solution steps was dependent on the W/H ratio; pillars with higher W/H ratio required a higher number of steps.

In MATLAB, the data was then superimposed on a multi-layered mesh whose nodal points coincided with the gridpoints in the FLAC^{3D} model. Three data acquisition functions with user-defined spatial limits helped in determining the evolution of applied strain, stress and plastic strains within the pillar. To compute the average strain for every set of datapoints (every set corresponds to a particular solution step), the average absolute displacements at the top and the bottom of the pillar were added and divided by the height of the pillar i.e. 8 m. Figure 5 shows the global stress-strain curves for W/H ratio of 1, 2 and 3.

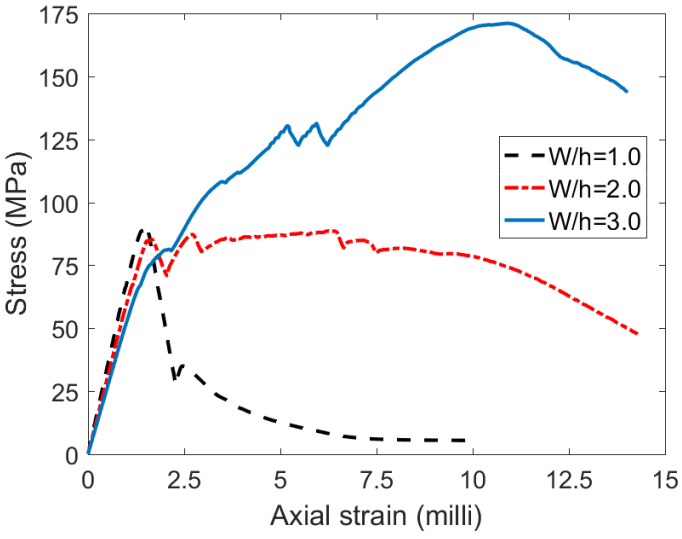

Figure 5: Average stress-strain curve for pillars with W/H of 1, 2 and 3.

Three important observations can be readily made in examining Figure 5: a) There is some amount of nonlinearity in the stress-strain curve prior to the peak strength; b) As the W/H ratio increases, the post peak behavior transitions from brittle to ductile; c) There is a minimal change in the strength between W/H of 1 and 2 and a drastic increase for W/H of 3. The brittle-ductile transition and higher strength corresponding to larger W/H ratio has been previously demonstrated in laboratory tests [39,40].

Interestingly, the model with W/H ratio of 2 and 3 continues to carry load even after achieving its peak strength. This could have major implications for support design for mine pillars. It is a common practice to assess support requirements on the sole basis of the estimated peak strength of pillars. If indeed the wider pillars could take on more deformation and dissipate energy from the system in a stable manner, then the support requirements could potentially be significantly reduced; conversely, the support density could be kept constant and the pillars could be made smaller, improving the production of the mine.

Figures 6 and 7 show the concentration of stresses around the core of the pillar for W/H of 2 and 3. As explained by Krauland and Soder [13], spalling type failure initiates along the periphery followed by channeling of excess load through the central portion of the pillar. A similar behavior was seen in the models where the excess load is channeled in a typical hour-glass shape. The difference in the lateral spread of the hour-glass reflects the higher load carrying capacity of squat pillars.

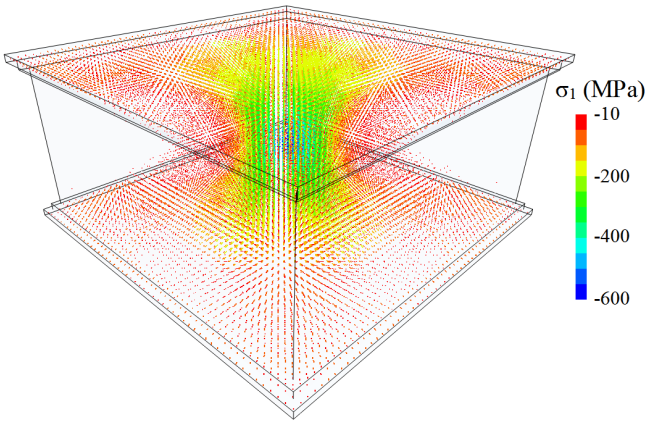

Figure 6: Concentration of vertical stress around the core of the pillar with W/H of 2.

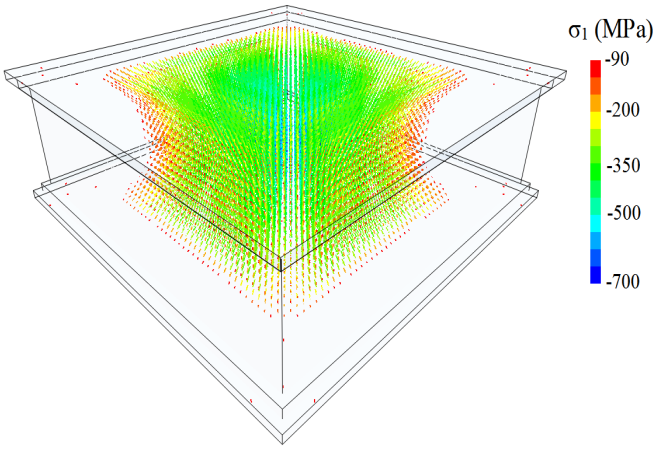

Figure 7: Concentration of vertical stress around the core of the pillar with W/H of 3.

The previous figures correspond only to the last solution step of the simulations but do not provide a visualization of the gradual development of stress as the model is subjected to incremental strain. Wagner [38] made an attempt to investigate this boundary-relaxation-core-loading phenomenon in the field by monitoring the gradual development of stress using hydraulic jacks installed across the mid-section of a coal pillar. Similar plots along the central plane of the pillar for W/H ratio of 3 were developed and are shown in Figure 8. This clearly illustrates the peripheral yielding process followed by the localization of stress through the pillar core. The figure is also in excellent correspondence with the field results of Wagner [38].

It is noteworthy to mention here that the peak stress carried by the pillar core is about 3.5-4 times the global peak strength obtained from the stress-strain curve. Although this might initially seem counter-intuitive, it can be explained by examining the plastic strains and corresponding confinement levels. Figure 9 presents a surface plot of the σ_1, σ_3 and eps along a horizontal central plane (W/h=3 pillar) for a solution step corresponding to an average strain value of 0.0085 (see Figure 5). With increasing damage (i.e. eps), dilation is mobilized generating some amount of lateral plastic strain. The localization of damage occurs first along the boundary due to lower confinement (resulting in lower strength and subsequent yield). Since the elements in the pillar are confined within this damaged zone, the lateral plastic strains increase the level of confinement near the pillar core, pushing the load carrying capacity of these elements

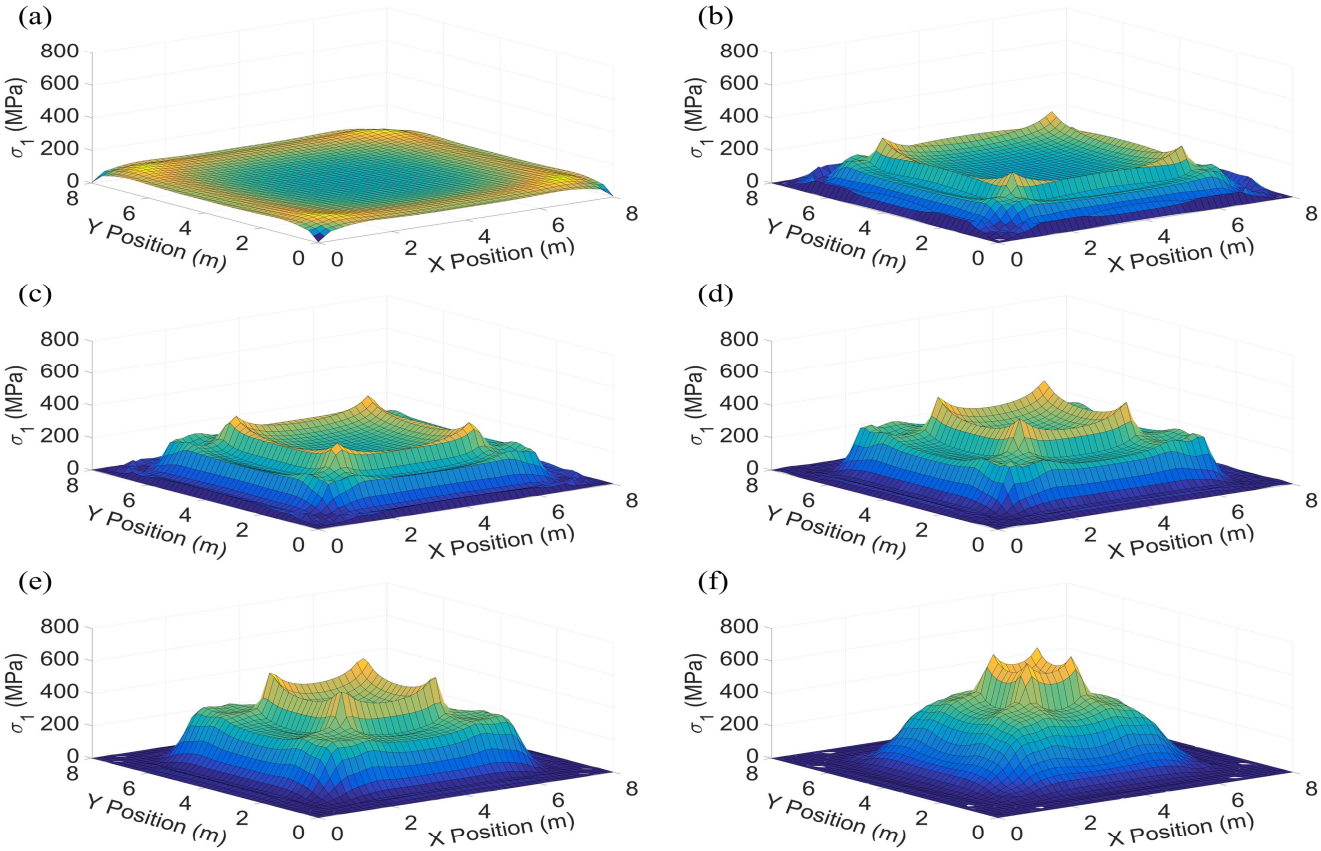

Figure 8: Development of vertical stress along the mid-height of the pillar with increasing damage to the system.

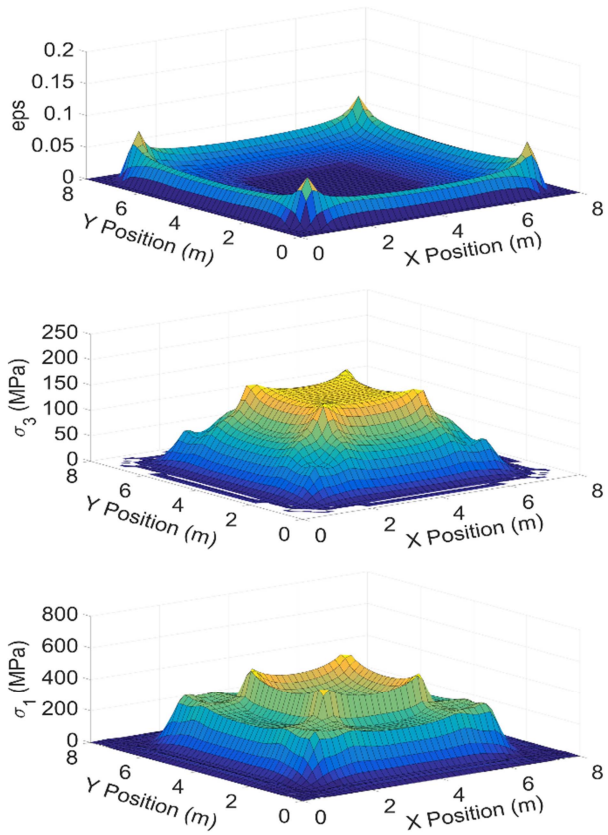

Figure 9: Plastic strain, confinement and vertical stress along the mid-height of the pillar (W/H=3) for a particular solution step

upward along the bilinear envelope. This is a progressive phenomenon where the zone of damage and dilatancy moves inward towards the pillar core as the system is perpetually strained until the system collapses completely.

5.0 ANALYSIS OF EXISTING PILLAR DATABASE AND MODEL PREDICTION

Over the years, numerous pillar strength curves have been established which provide rough estimates of the strength of pillars as a function of the W/H ratio and UCS. These curves were drawn by fitting boundaries between failed and stable pillar case histories documented in literature. A major concern in some of these studies is the fact that a variety of rocks with significantly different strength properties were considered before segregating the datasets. Such an approach may inappropriately combine the behavior of several rock types with different mechanical characteristics. To eliminate this issue in comparing available empirical data to the models run as part of this study, all the available datasets were combined to make a database and then filtered to include only cases with a rock UCS exceeding 200 MPa. The choice of UCS value was driven by the scope of this current work (i.e. hard rocks similar to the Creighton Granite). Only the datasets of Hudyma [41], Hedley and Grant [21] and Sjoberg [23] satified the selection criteria.

Each of these three studies suffer from some kind of drawback. In Hudyma [41] and Sjoberg [23], the stresses were calculated using a 2-D displacement discontinuity software with an elastic constitutive model. It has already been demonstrated that there is some amount of non-linear behavior in the pre-peak portion of the stress-strain curve. Moreover, the classification of whether the pillar is stable or not was made by on-site staff which could have been highly subjective. The Hedley and Grant [21] study used a modified tributary area theory which also considers only elastic behavior. It could be concluded that the datapoints maybe associated with some errors and may not reliably represent the actual pillar strengths. However, very limited information is provided in literature regarding these case studies which renders revaluation of the reliabiliy of the datasets impossible.

The filtered dataset is presented graphically in Figure 10. The black line which delineates the failed and stable pillar cases represents the pillar strength envelope. The pink line indicates the locus of the peak strength as obtained from the models presented in this study. Some of the important conclusions that can be drawn are as follows:

- The modeled strength curve does not increase exponentially beyond W/H=2 as in the cases of Martin and Maybee [14] and Mortazavi et al. [15] for rocks with UCS>200 MPa. There is some amount of strength increase in the models with W/H>2, although the overall convex shape of this trend is consistent with what has historically been associated with this type of relationship.
- Minimal data (specifically unstable and failed pillar cases) is available for W/H>2. No conclusion can be derived from the database regarding behavior of squat pillars in very strong rock, although the modeled results are consistent with the data that are available.
- For pillars with W/H<1, a straight line with very low slope is more representative for strong rocks. Generally speaking, a slender pillar has inadequate width to generate a highly confined core, and as a result, strength increase is unlikely.
- The modeled strength curve matches closely with the line fitted to the empirical database. Only the y-intercept of the two lines are slightly offset. The authors believe that this may be either due to the non-linearity of the scaling factor for eps in FLAC^{3D} or the monotonic loading scheme applied to the models. The effect of both of these factors are currently being evaluated to obtain a better fit to the empirical curve.

6.0 CONCLUSION AND RECOMMENDATION

This study has presented a local constitutive relationship for hard rock pillars that has the capability of capturing microscopic damage processes while exhibiting an emergent pillar behavior consistent with what has been observed in the field. Numerical models of pillar loading successfully demonstrated the hour-glass shape of the core and the progressive localization of stress along the mid-section. These observations are in correspondence to Krauland and Soder [13] and Wagner [38].

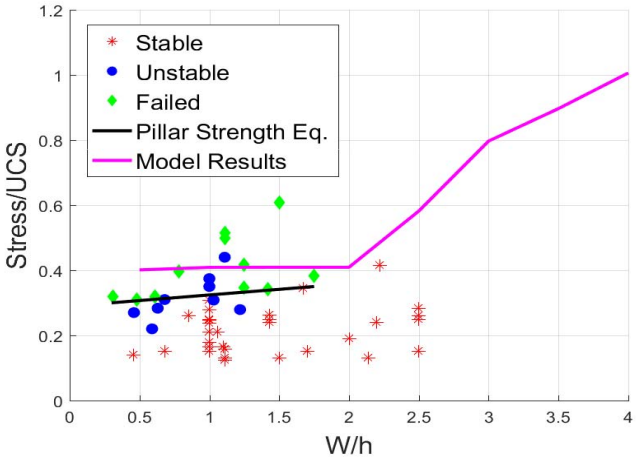

Figure 10: Plot of stable, unstable and failed case histories (Black line indicates an approximate demarcation between the unstable and failed pillars; pink line represents a fit to the model results).

The progressive S-shaped strength criterion presented in this work captures extensile-spalling behavior in low confinement areas and shear based failure in high confinement areas with consideration of the progressive damage process. The implementation of the progressive S-shaped criterion is relatively simple in FLAC^{3D}. The issue lies in determining the parameters, which are based on CI, CD and spalling limits for a particular rock. For the most part, the required parameters can be determined from laboratory testing on rock samples. In the case where such testing is not possible, the reader can refer to the guidelines proposed by Walton [42] as a starting point followed by calibration of the most uncertain parameters to achieve a better fit to field measurements.

Numerous pillar strength curves relating the normalized peak strength to the W/H ratio have been proposed in literature over the past few decades. Neglecting the methodology followed in deducing each of the datapoint, most of the curves were developed considering a wide variety of rocks with significantly different UCS. Such a classification may not accurately explain the behavior of pillars within a particular rock type. In this study, the database has been segregated based on UCS. It is evident that for the strongest rocks, there is only a modest increase in pillar strength for W/H ratio up to 2. The bilinear model was shown to closely match this trend and also predicted an increase in strength beyond W/H of 2. Overall, the envelope developed in this study was successful in representing the behavior of hard rock pillars.

ACKNOWLEDGEMENTS

The research conducted for this study was funded by the National Institute of Occupational Health and Science (NIOSH) under Grant Number 200-2016-90154. The authors would like to extend their sincere gratitude for this financial support.

REFERENCES

1. Esterhuizen, G.S., D.R., Dolinar and J.L., Ellenberger. 2011. Pillar strength in underground stone mines in the united states. *International Journal of Rock Mechanics and Mining Sciences*, 48:42–50.
2. Hoek, E., P.K., Kaiser and W.F., Bawden. 1995. *Support of underground excavation in hard rock*. A.A. Balkema, Rotterdam, p. 215.
3. Diederichs, M.S. 2003. Rock fracture and collapse under low confinement conditions. *Rock Mechanics and Rock Engineering*, 36:339-381.
4. Diederichs, M.S. 2007. The 2003 geotechnical colloquium: Mechanistic interpretation and practical application of damage and spalling prediction criteria for deep tunnelling. *Canadian Geotechnical Journal*, 44:1082-1116.
5. Diederichs, M.S., P.K., Kaiser. and E., Eberhardt. 2004. Damage initiation and propagation in hard rock during tunnelling and the influence of near-face stress rotation. *International Journal of Rock Mechanics and Mining Sciences*, 41:785-812.
6. Martin, C.D. 1997. Seventeenth Canadian geotechnical colloquium: The effect of cohesion loss and stress path on brittle rock strength. *Canadian Geotechnical Journal*, 34:698-725.
7. Martin, C.D., P.K., Kaiser and D.R., McCreath. 1999. Hoek-Brown parameters for predicting the depth of brittle failure around tunnel. *Canadian Geotechnical Journal*, 36:136-151.
8. Martin, C.D. and N.A., Chandler. 1994. The progressive fracture of Lac Du Bonnet granite. *International Journal of Rock Mechanics and Mining Sciences and Geomechanical Abstracts*, 31:643-659.
9. Pelli, F., P.K., Kaiser and N.R., Morgenstrern. 1991. An interpretation of ground movements recorded during construction of the Donkin-Morien tunnel. *Canadian Geotechnical Journal*, 28:239-254.
10. Hajiabdolmajid, V., P.K., Kaiser and C.D., Martin. 2002. Modelling brittle failure of rock. *International Journal of Rock Mechanics and Mining Sciences*, 39:731-341.

11. Schmertmann, J.H. and L.O., Osterberg. 1960. An experimental study of the development of cohesion and friction with axial strain in saturated cohesive soils. *Research Conference on Shear Strength of Cohesive Soils*, Boulder, CO. 643-694.
12. Walton, G. 2014. *Improving continuum models for excavations in rock masses under high stress through an enhanced understanding of post-yield dilatancy.* Ph.D. Thesis. Queen's University, Kingston, Canada, 2014.
13. Krauland, N. and P.E., Soder. 1987. Determining pillar strength from pillar failure observation. *Engineering Mining Journal*, 8:34-40.
14. Martin, C.C. and W.G., Maybee. 2000. The strength of hard rock pillar. *Int J Rock Mec Min Sci*, 37:1239-1246.
15. Mortazavi, A., F.P., Hassani and M., Shabani. 2009. A numerical investigation of rock pillar failure mechanism in underground openings. *Computer and Geotechnics*, 36-5:619-697.
16. Walton, G., M.S., Diederichs and A. Punkkinen. 2015. The influence of constitutive model selection on predicted stresses and yield in deep mine pillars-A case study at the Creighton mine, Sudbury, Canada. *Geomechanics and Tunneling*, 5:441-449.
17. Walton, G. and M.S. Diederichs. 2015. A new model for the dilation of brittle rocks based on laboratory compression test data with separate treatment of dilatancy mobilization and decay. *Geotechnical and Geological Engineering,* DOI:10.1007/s10706-015-9849-9.
18. Kaiser, P.K., B., Kim, R.P. Bewich and B., Valley. 2011. Rock mass strength at depth and implication for pillar design. *Mining Technology*, 120(3):170-179.
19. Kaiser, P.K. and B., Kim. 2015. Characterization of strength of intact brittle rock considering confinement-dependant failure processes. *Rock Mech Rock Eng*, 48:107-119.
20. Salamon, M.D.G. and A.H., Munro. 1967. A study of the strength of coal pillars. *J. South African Inst. Min. Metall.*, 68: 55-67.
21. Hedley, D.G.F. and F., Grant. 1972. Stope and pillar design for the Elliot Lake uranium mines. *Can. Inst. Min. Metall. Bull*, 65:1165-1186.
22. Lunder, P.J. and R., Pakalnis. 1997. Determining the strength of hard rock mine pillars. Bull. *Can. Inst. Min. Metall.,* 90:51-55.
23. Sjoberg, J. 1992. Failure modes and pillar behavior in the Zinkgruvan mine. Proc *33rd U.S. Rock Mechanics Symposium*, pp 491-500.
24. Potvin, Y., M., Hudyma and H.D.S., Miller. 1989. Rib pillar design in open stoping. *Can. Inst. Min. Metall. Bull.*, Vol 82:31-36.
25. Edelbro, C. 2009. Numerical modelling of observed fallouts in hard rock masses using an instantaneous cohesion-softening friction-hardening model. *Tunnelling and Underground Space Technology*, 24:398-409.
26. Walton, G., M.S., Diederichs, L.R., Alejano and J., Arzua. 2014. Verification of a laboratory-based dilation model for insitu conditions using continuum models. *J Rock Mech and Geotech. Engr.*, 6:522-534.
27. Zhao, X., M., Cai and M., Cai. 2010. Consideration of rock dilation on modeling failure and deformation of hard rocks- a case study of the mine-by test tunnel in Canada. *J Rock Mech and Geotech. Engr.*, 2(4):338-349.
28. Ebarhardt, E., D. Stead, B., Stimpson and R., Read. 1998. Identifying crack initiation and propagation thresholds in brittle rocks. *Can Geotech J*, 35(2): 222-233.
29. Brace, WF., B., Paulding and C., Scholz. 1966. Dilatancy in the fracture of crystalline rocks. *J geophysics Res*, 71:3939-3953.
30. Lajtai. EZ. 1974. Brittle fracture in compression. *Int J Fract Mech*, 10:525-536
31. Nicksiar, M. and C.D., Martin. 2012. Evaluation of methods for determining crack initiation in compression tests on low-porosity rocks. *Rock Mech Rock Eng*, 45:607-617.
32. Walton, G., A., Hedayat, E., Kim and D., Labrie. 2017. Post-yield strength and dilatancy evolution across the brittle-ductile transition in Indiana Limestone. *Rock Mech Rock Eng*. Under Revision.
33. Mogi, K. 1966. Pressure dependence of rock strength and transition from brittle fracture to ductile flow. *Bulletin of the Earthquake Research Institute*, 44:215-232.
34. Walton, G. and M.S., Diederichs. 2015. Dilation and post-peak behavior inputs for practical engineering analysis. *Geotechnical and Geological Engineering*, DOI 10.1007/s10706- 014-9816-x.
35. Zhao, X.G. and M., Cai. 2010. A mobilized dilation angle model for rocks. *Int J Rock Mech Min Sci*, 47:368-384.
36. Alejano, L.R. and E., Alonso. 2005. Consideration of dilatancy angle in rock and rock masses. *Int J Rock Mech Min Sci*, 42:481-507.
37. Anon. 2016. FLAC 3D Example Application Version v6. Itasca Consulting Group, Minneapolis, Minnesota.
38. Wagner, H. 1974. Determination of the complete load-deformation characteristics of coal pillars. *3rd Congress*, ISRM, Denver, Co. 1067-1081.
39. Das, M.N. 1986. Influence of width/height ratio on post-failure behavior of coal. *Int J Min Geological Eng,* 4:79-87.
40. Hudson, J.A., E.T., Brown and C., Fairhurst. 1971. Shape of the complete stress-strain curve for rock. *Proc Symp. Rock Mech. 13th,* Univ Illinois, Urbana,IL.
41. Hudyma, M.R. 1988. *Rib pillar design in open stope mining*. M.A.Sc. Thesis, The University of British Columbia.
42. Walton, G. 2017. Guidelines for the selection of input parameters for Cohesion-Weakening-Friction-Strengthening (CWFS) analysis of excavations in brittle rock. *Rock Mech Rock Eng.* Submitted.